Original Article

JCBFM

Journal of Cerebral Blood Flow & Metabolism
2018, Vol. 38(5) 835–846

DOI: 10.1177/0271678X17703888
journals.sagepub.com/home/jcbfm
SAGE

Overexpression of VLA-4 in glial-restricted precursors enhances their endothelial docking and induces diapedesis in a mouse stroke model

Anna Jablonska[1,2], Daniel J Shea[3], Suyi Cao[1,2], Jeff WM Bulte[1,2,3,4,5], Miroslaw Janowski[1,2,6], Konstantinos Konstantopoulos[3] and Piotr Walczak[1,2,7]

Abstract

The loss of oligodendrocytes after stroke is one of the major causes of secondary injury. Glial-restricted progenitors (GRPs) have remylenating potential after intraparenchymal cerebral transplantation. The intraarterial (IA) injection route is an attractive gateway for global brain delivery, but, after IA infusion, naive GRPs fail to bind to the cerebral vasculature. The aim of this study was to test whether overexpression of Very Late Antigen-4 (VLA-4) increases endothelial docking and cerebral homing of GRPs in a stroke model. Mouse GRPs were co-transfected with DNA plasmids encoding VLA-4 subunits (α4, β1). The adhesion capacity and migration were assessed using a microfluidic assay. In vivo imaging of the docking and homing of IA-infused cells was performed using two-photon microscopy in a mouse middle cerebral artery occlusion (MCAO) model. Compared to naïve GRPs, transfection of GRPs with VLA-4 resulted in >60% higher adhesion ($p < 0.05$) to both purified Vascular Cell Adhesion Molecule-11 (VCAM-11) and TNFα-induced endothelial VCAM-1. VLA-4$^+$GRPs displayed a higher migration in response to a chemoattractant gradient. Following IA infusion, VLA-4$^+$GRPs adhered to the vasculature at three-fold greater numbers than naïve GRPs. Multi-photon imaging confirmed that VLA-4 overexpression increases the efficiency of GRP docking and leads to diapedesis after IA transplantation. This strategy may be further exploited to increase the efficacy of cellular therapeutics.

Keywords

Stroke, cell transplantation, adhesion molecules, white matter/oligodendrocytes, two-photon microscopy

Received 10 August 2016; Revised 27 February 2017; Accepted 12 March 2017

Introduction

Stroke is a leading cause of long-term, severe disability worldwide and, to date, most patients cannot receive effective treatment.[1,2] Stroke usually originates from the sudden occlusion of a vessel carrying blood to the brain, resulting in an almost immediate loss of oxygen and energy supply,[3,4] and, depending on the occlusion site, the lesion can encompass the white or gray matter, or both.[5] Oligodendrocyte survival and preservation of

[1]Russell H. Morgan Department of Radiology and Radiological Science, The Johns Hopkins University School of Medicine, Baltimore, USA
[2]Institute for Cell Engineering, Cellular Imaging Section, The Johns Hopkins University School of Medicine, Baltimore, USA
[3]Department of Chemical & Biomolecular Engineering, The Johns Hopkins University Whiting School of Engineering, Baltimore, USA
[4]Department of Biomedical Engineering, The Johns Hopkins University School of Medicine, Baltimore, USA
[5]Department of Oncology, The Johns Hopkins University School of Medicine, Baltimore, USA
[6]NeuroRepair Department, Mossakowski Medical Research Centre, Warsaw, Poland
[7]Department of Radiology, University of Warmia and Mazury, Olsztyn, Poland

Corresponding author:
Piotr Walczak, Associate Professor, Russell H. Morgan Department of Radiology and Radiological Science, Division of MR Research Institute for Cell Engineering, Johns Hopkins University School of Medicine, Broadway Research Building, Rm 647, 733 N Broadway, Baltimore, MD 21205, USA.
Email: pwalczak@mri.jhu.edu

myelin integrity is critical to normal axonal function. However, the vulnerability of oligodendrocytes to ischemic injury has been demonstrated in numerous in vitro and in vivo studies.[6–10] The first signs of oligodendrocyte destruction, as measured by the degradation of basic myelin protein (MBP), is visible as soon as 24 h after stroke onset,[11] followed by a massive loss of oligodendrocytes at 48 h.[12] This loss and dysfunction of oligodendrocytes can cause significant secondary axonal injury.[13]

Recent evidence suggests that stem cell-based therapy is a viable option for the restoration of destroyed oligodendrocytes. For instance, transplantation of oligodendrocyte progenitors can lead to improved myelination in animal models of multiple sclerosis[14] or spinal cord transaction.[15] Glial-restricted progenitors (GRPs) are a viable source of highly therapeutic myelinating oligodendrocytes, and, following transplantation into the focally demyelinated spinal cord of adult rats or into the brain of neonatal dysmyelinated shiverer mice,[16,17] GRPs can migrate extensively and differentiate into mature oligodendrocytes. However, the efficiency and safety of GRP delivery into the injured brain, including transient ischemia, remains unknown.

Intraparenchymal injection, although used frequently in (pre-)clinical studies, is invasive and results in a relatively small biodistribution area, which represents a significant drawback when targeting large lesions, including those occurring in stroke. Intravenous (IV) cell delivery is an attractive alternative and is being extensively used in preclinical[18–20] and clinical[21,22] settings for stroke treatment. Although IV injection is less invasive, most of the transplanted cells are trapped in the filtering organs, including the lung, liver, spleen, and kidney.[23,24] As a result, only a small fraction of injected cells reaches the brain. Less conventional cell delivery methods, such as intraperitoneal,[25] intracardiac,[26] and intranasal,[27] have been used, with minimal success, thus failing to justify their broad application. However, a promising yet challenging administration route is intraarterial (IA) injection. Transplantation of cells directly into the artery has the advantage of selectively targeting cells to large areas of the injured brain, bypassing the peripheral filtering organs.[28,29] While intraarterial infusion of large-size mesenchymal stem cells may lead to complications,[30,31] the delivery of even large quantities of small-size GRPs is safe.[32] The potential clinical use of IA injection requires that cells effectively bind to the brain endothelium, as they otherwise would pass through the brain and ultimately be deposited in the filtering organs, as in the case of IV injection.

To ensure effective endothelial capture, injected cells must express key integrins that facilitate their binding with endothelial counterparts. The integrin Very Late Antigen-4 (VLA-4, a heterodimer of integrin α4 and β1) and its ligand Vascular Cell Adhesion Molecule-1 (VCAM-1) is a well-characterized receptor-ligand pair involved in leukocyte trafficking, including cell diapedesis into the brain parenchyma.[33] Since increased VCAM-1 expression on the endothelium has been detected following stroke injury,[34,35] VLA-4 may be potentially exploited as a docking molecule on the cell membrane. Indeed, neural stem cells enriched for VLA-4 expression display enhanced homing to the infarcted brain.[36] Native GRPs do not express VLA-4; however, VLA-4 expression can be induced via genetic engineering. As proof-of-principle, we showed previously that overexpression of VLA-4 in immortalized GRPs can be successfully used to enhance cerebral endothelial binding in an LPS-induced inflammatory brain model.[37] In this study, we developed a multi-faceted platform where the interaction between VLA-4$^+$GRPs and VCAM-1 was first assessed in vitro using microfluidic assays to measure cell binding under shear flow conditions. Moreover, we demonstrate here efficient IA delivery and diapedesis of primary VLA-4$^+$GRPs to the ischemia-injured brain parenchyma in vivo, as demonstrated by intravital two-photon microscopy (2-PM).

Materials and methods

Derivation and maintenance of GRPs

Primary mouse GRPs were isolated from the brain of E13 mouse embryos as described.[38] Cells were maintained in Dulbecco's modified Eagle's medium, nutrient mixture F-12 (Life Technologies), supplemented with basic-FGF (basic fibroblast growth factor), B-27, and N2 (Life Technologies), seeded on poly-L-lysine (PLL)/laminin (Sigma)-coated dishes, and cultured in 5% CO_2 and ambient oxygen for up to three passages.

Cell labeling

Native GRPs and VLA4$^+$GRPs were labeled with the fluorescent dye CellTracker^{TM} Green CMFDA (Life Technologies). Cells were incubated at 37°C with 25 μM CMFDA for 30 min. After that time, cells were washed 3 times with PBS and resuspended in PBS at the required concentration.

VLA-4 transfection

Three days prior to cell infusion, GRPs were seeded at a density of 1×10^5 cells/cm^2 and co-transfected with the α4 and β1 subunits of VLA-4 integrin (GeneCopoeia, 2,4 ng/mL) using Lipofectamine 2000 (Life Technologies, 4 μL/mL). VLA-4 expression was confirmed with immunohistochemical staining for

each integrin subunit (human integrin alpha 4/CD49d: R&D Systems; integrin β1 (N-20): Santa Cruz Biotechnology) and with RT-PCR. On the day of transplantation, cells were harvested using Accutase (Sigma), and resuspended in PBS at 2×10^6 cells/ml.

Differentiation assay

VLA-4-transfected GRPs were seeded in 24-well plates at a density of 1×10^4 cells/cm^2. Forty-eight hours after transfection, the maintenance medium was supplemented with Triiodo-L-Thyronine T3 (Sigma, 40 μg/ml) to induce oligodendrocyte differentiation. After 6 days of culture, cells were fixed with 4% paraformaldehyde (PFA) for immunocytochemistry (anti-myelin basic protein (MBP), Santa Cruz) or collected for RT-PCR (MBP, Olig2, glial fibrillary acid protein (GFAP)).

RT-PCR assay

Cellular mRNA was isolated from the cells using Trizol according to the manufacturer's instructions (BioRad). For cDNA synthesis, a RNA-to-cDNA Reverse Transcriptase Kit (Ambion) was used. Primers for the integrin subunits α4 and β1, as well as for other selected genes (MBP, Olig2, and GFAP), were designed using Primer3 and Blast software.

Microfluidic assays

Flow-based adhesion assays were performed in a microfluidic device, as previously described.[39,40] Pure VCAM-1 or endothelial cells were used as a substrate for this flow-based adhesion assay. The dimensions of the microchannels were $L \times W \times H = 2000 \times 500 \times 20$ μm (VCAM1-coated) or $2000 \times 500 \times 40$ μm (HBEC-coated). A shear stress of 1 dyn/cm^2 was used throughout all experiments. On the day of the experiment, 50 μl of 1×10^6 cells/ml (naïve GRPs or VLA4 + GRPs) in D-PBS containing 0.1% bovine serum albumin (BSA) were loaded on the inlet of the microfluidic device. A 20× objective with a field of view of 950×725 μm^2 was used to monitor cell binding under shear flow. Each perfusion experiment lasted 3 min. Cell velocities were determined by dividing the distance the cell traveled during cell-substrate interaction by the time for each tested condition.[41]

Preparation of microfluidic devices coated with endothelial cells

A pre-cleaned glass slide and a microfluidic device were plasma-treated for 2 min and adhered together to create a seal. Channels were perfused with 20 μg/ml fibronectin (Sigma) and incubated for 1 h at 37°C. Fibronectin was removed by washing with D-PBS. Human brain endothelial cells (HBEC, 2×10^6 cells/ml) were perfused into the channels and incubated at 37°C for 48 h, with changing of media every 12 h to allow adhesion of HBECs. Twenty-four hours prior to the onset of the flow experiments, endothelial cells were activated by exposure to 40 ng/ml TNFα (Cell Signaling Technology).

Chemotaxis migration assay

A migration assay was performed in chemoattractant gradient-generating devices fabricated as described previously.[42–44] A total of 50 μL of 5×10^6 cells/ml was added to the inlet of the microfluidic device. Cell migration was visualized using a bright-field microscope (Nikon, Japan) every 20 min for 16 h with the NIS-Elements software. Migration velocity was analyzed using the NIS-Elements add-on Tracking module. Data represent the mean ± S.D. values of five independent experiments.

Induction of stroke model

Experiments were performed in accordance with guidelines for the care and use of laboratory animals approved by the Institutional Animal Care and Use Committee of Johns Hopkins University, designed in compliance with the Animal Welfare Act regulations and Public Health Service (PHS) Policy. All animal experiments were approved by The Johns Hopkins Institutional Animal Care and Use Committee and were in compliance with ARRIVE guidelines. Ischemia was induced in adult male SVE 129 and NOD-SCID mice (Jackson Labs) using a transient middle cerebral artery occlusion (MCAO) model.[45] Animals were housed in the Johns Hopkins School of Medicine animal facility in standard cages with filter tops, with a 12:12 light:dark cycle, controlled humidity and temperature conditions, and with ad libitum access to water and food. Briefly, animals were anesthetized with 1–2% isofluorane in oxygen-enriched air using a face-mask. A small scalp incision was made and a small parietal burr hole was made with a low-speed drill until a thin amount of bone remained. A small laser Doppler probe (Moor Instruments, USA) was held against the bone for cerebral blood flow measurements. The right common carotid artery was exposed through a side neck incision. The right external carotid artery was ligated proximal to the occipital artery, the occipital artery was cauterized, and the pterygopalatine artery was ligated. An incision was made in the common carotid artery distal to the ligation and an occluding filament was advanced into the internal carotid artery (ICA) to the origin of the MCA, a point at which the

laser Doppler signal abruptly drops. Reduction of signal was 70% of baseline and the MCAO was maintained for 1 h, after which the neck incision was closed with sutures.

IA infusion of GRPs

One day after MCAO, animals were anesthetized with 1–2% isofluorane in oxygen-enriched air using a facemask. The right ICA was exposed through a side neck incision. Animals were randomly assigned to control (naïve GRPs; $n = 5$ for 2PM study and $n = 3$ for long-term 30-day follow-up study) and experimental ($VLA4^+$GRPs; $n = 5$ for 2PM study and $n = 3$ for long-term 30-day follow-up study) groups. A dedicated mouse carotid artery catheter (Instech) was placed in the ICA and its position was fixed with two sutures. Cell infusion was performed after placing anesthetized animals in a custom-made frame during the course of 2-PM. The cell suspension (1×10^6 cells in 200 µl PBS) was infused over 5 min using an automated infusion pump.

Intravital 2-PM

All animal procedures were reviewed and approved by the Johns Hopkins Animal Care and Use Committee. Intravital imaging was performed with an Olympus FV1000MPE multiphoton laser-scanning microscope. On the day of imaging, animals were anesthetized with 1–2% isofluorane in oxygen-enriched air. A small scalp incision was made and a skull window ($2 \times 2\,mm^2$) was made above the right hemisphere with a high-speed drill. The exposed brain was cleaned with saline to remove any blood. A custom-made head post was cemented to the skull and the animal was placed in a custom-made frame to eliminate respiratory motion. TexasRed conjugated dextran (Mw = 70 kDa, Life Technologies) was injected via an ICA catheter 10 min before cell infusion to visualize blood vessels. GRPs were then injected over 1 min and the selected field of view was imaged every 10 min for 3 h ($n = 5$ for the control and experimental groups). After imaging, animals were sacrificed and brains were collected for further analysis.

Histopathological analysis

After intravital imaging, mice were perfused with 4% PFA. Brains were removed and cryopreserved in 20% sucrose for 48 h, frozen on dry ice, and cryosectioned as 20 µm coronal sections. Tissue sections were examined with an Axio Vert inverted microscope and tiling module (Zeiss). The number of green fluorescent cells (CMFDA-labeled) in the ipsilateral hemisphere was counted for both the experimental and control groups ($n = 5$ each), with four random brain slices each, resulting in a total number of 20 counts per group.

NOD-SCID animals transplanted with naïve or $VLA4^+$GRPs were sacrificed 30 days after cell transplantation. Animals were perfused with 4% PFA, brains were removed, cross-sectioned at 20 µm, and processed for fluorescence microscopy. Tissue sections were imaged with an Axio Vert inverted microscope to detect GFP-expressing transplanted GRP cells.

Statistical analysis

Data are presented as mean ± 95% confidence interval (CI) for $n \geq 4$ independent experiments. The statistical significance of differences between groups was tested with a non-parametric Kruskal–Wallis test for the comparison of multiple groups (transfection efficiency, microfluidic assays) or the Mann–Whitney test for pairwise comparison of naïve and $VLA4^+$GRPs groups (microfluidic assays, migration assay, and histopathology). All calculations were performed using Prism 3.0, with $p < 0.05$ considered significant. To identify minimum differences (considered as clinically relevant), the Hedges' g factor was calculated. For this exploratory study, all tests were two-sided, with no further adjustment for multiple comparisons.

Results

Characterization of $VLA\text{-}4^+$GRPs

Expression of both the α4 and β1 integrin subunits in transfected GRPs was confirmed with RT-PCR and immunocytochemistry. Immunostaining showed that 66% and 70% of the cells were positive for integrin α4 and β1 subunits, respectively (Figure 1(a) and (b)). Non-transfected GRPs were negative for the expression of both VLA-4 subunits. VLA-4 expression did not affect the differentiation of GRPs toward mature oligodendrocytes, as demonstrated by the presence of the mature oligodendrocyte marker MBP at the mRNA and protein levels (Figure 1(d)).

Binding of $VLA\text{-}4^+$GRPs to purified VCAM-1

Overexpression of VLA-4 in GRPs resulted in a markedly higher binding capacity to the purified VCAM-1 substrate, compared to controls, accompanied by a significantly lower cell velocity attributed to the formation of VLA4-VCAM-1 bonds, resulting in more resistance to dispersive hydrodynamic shear forces. The VCAM-1-bound $VLA\text{-}4^+$GRPs traveled at a speed of 17.9 (95% CI 15.6 to 20.3) µm/s, which was 72% lower than that measured for naïve GRPs (48.5 (95% CI

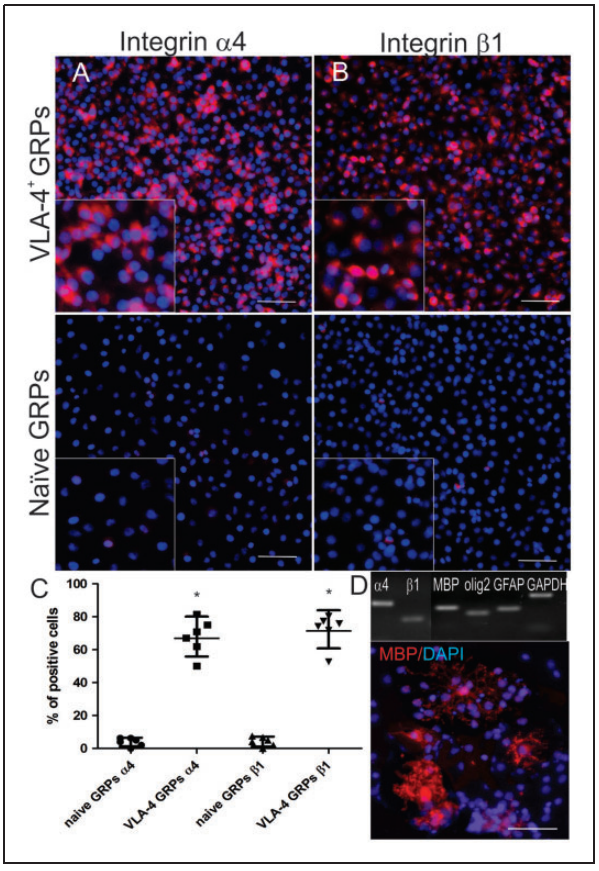

Figure 1. Assessment of transfection efficacy. Shown are immunostaining and the averaged proportions of cells (shown as a mean and 95% CI) expressing integrin α4 (a,c) and β1 (b,c). Differentiation of VLA-4$^+$GRP was confirmed by positive staining, as well as by RT-PCR, for the oligodendrocyte-specific proteins, Olig2 and myelin basic protein (MBP) (d). Statistical analysis was performed using the Mann–Whitney test. Scale bar = 100 μm.

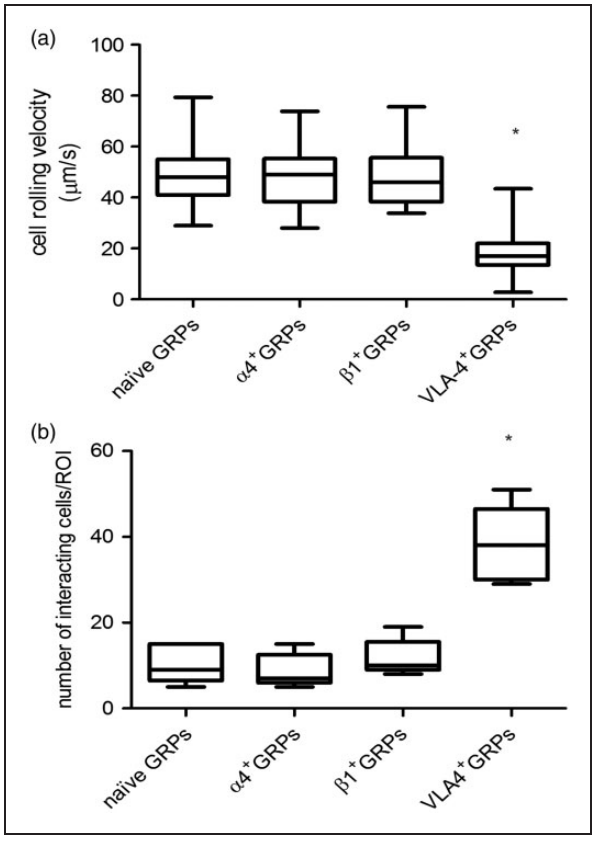

Figure 2. Binding of naïve GRPs and VLA-4$^+$GRPs to purified VCAM-1. Shown are the cell rolling velocity (a) and number of interacting cells (b) in the microfluidic channels coated with the VCAM-1 at a shear stress rate of 1 dyn/cm^2. Asterisk marks significant differences between the naïve and VLA-4$^+$GRPs. FOV = 160,000 μm^2; n = 5. Statistical analysis was performed using the Kruskal–Wallis test.

43.1 to 54.1) μm/s (p = 0.003, Hedges' g = 2.885)) (Figure 2(b)). Transfection of GRPs with only one single subunit of VLA-4 did not significantly alter cell velocity for naïve GRPs vs VLA-4$^+$GRPs (47.1 (95% CI 41.0 to 53.2; p = 0.960; Hedges' g = 0.11) vs. 48.6 (95% CI 42.5 to 54.6 μm/s; p = 0.960; Hedges' g = 0.001) for α4$^+$ and β1$^+$GRPs, respectively). As expected, the rolling of VLA-4$^+$GRPs was non-uniform and transient. The binding of VLA-4$^+$GRPs to VCAM-1 was non-static, with multiple short periods of cell arrest. Conversely, naïve GRPs, α4$^+$GRPs, and β1$^+$GRPs bound to VCAM-1 with 74% less efficiency compared to VLA-4$^+$ cells (Figure 2(a)). Evidently, transfection with both subunits of VLA-4 was necessary for cell binding and improved cell tethering to VCAM1-coated channels. We observed more than a 3-times higher number of interacting cells after the overexpression of VLA-4 (VLA-4$^+$GRPs 38.2 (95% CI 27.2 to 49.2; p < 0.001, Hedges' g = −3.578)) compared to naïve GRPs (10.4 (95% CI 4.9 to 15.9), α4$^+$GRP 8.8 (95% CI 3.6 to 13.6; p = 0.159, Hedges' g = 0.346) and β1$^+$GRP (11.8 (95% CI 6.5 to 17.1; p = 0.430, Hedges' g = 0.311)) (Figure 2(b)). Statistical analysis was performed with the Kruskal–Wallis test.

Binding of VLA-4$^+$GRPs to TNFα-activated, VCAM-1 expressing HBECs

Incubation of HBEC with TNFα increased the expression of VCAM-1, as demonstrated by immunocytochemistry (Figure 3(a) and (b)). Perfusion of cells through a microfluidic channel coated with activated HBECs showed a significantly lower (by 65%) average speed of VLA-4$^+$GRPs compared to naïve GRPs (Figure 3(c)) (VLA4$^+$GRPs 50.7 (95% CI 42.3 to 59.0) μm/s; naïve GRPs 146.7 (95% CI 118.5 to 174.9) μm/s; p < 0.001; Hedges' g = 2.884)). Such changes could not

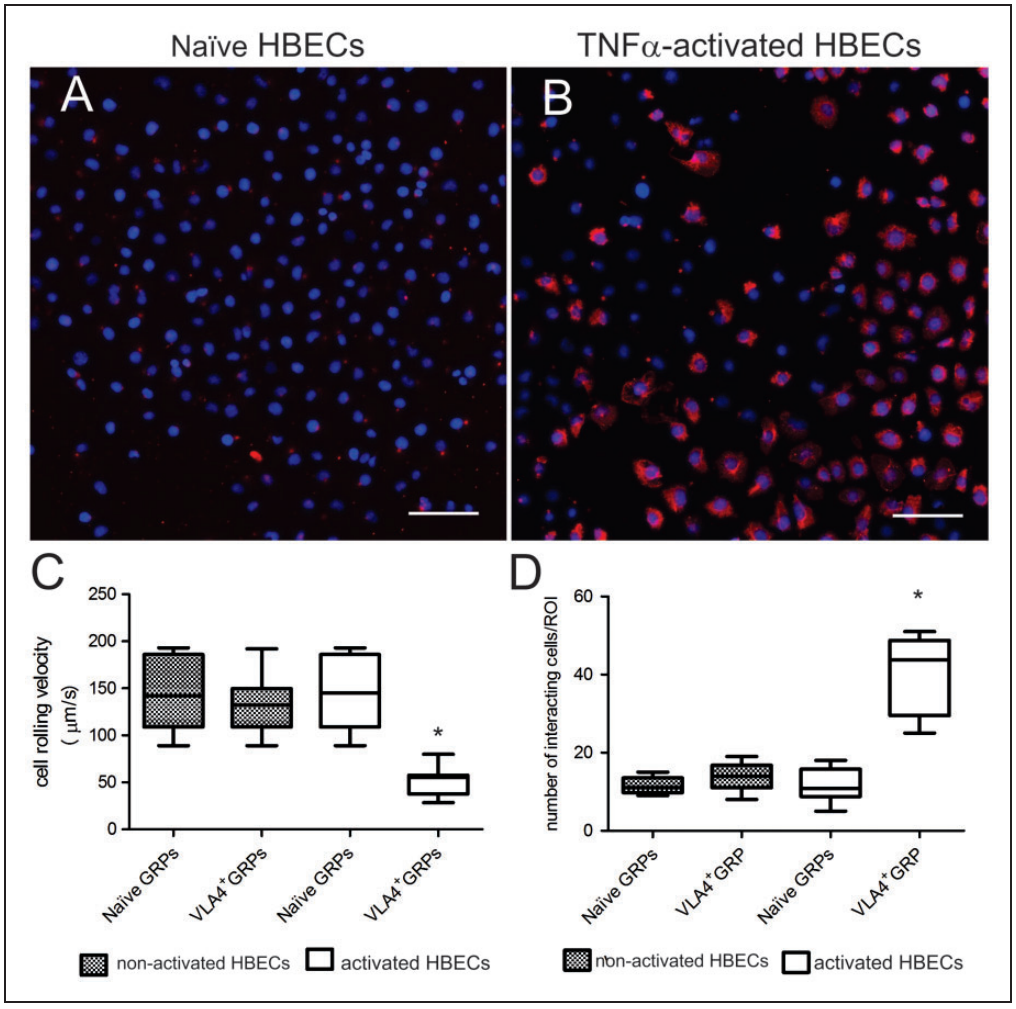

Figure 3. Binding of naïve GRPs and VLA-4$^+$GRPs in a microfluidic device coated with VCAM-1 expressing and non-expressing HBEC. Shown is the expression of VCAM-1 on non-activated (a) and TNFα-activated (b) HBECs. Cell rolling velocity (c) and number of interacting cells (d) were determined at a shear stress rate of 1 dyn/cm^2. Asterisk marks a significant difference between the naïve and VLA-4$^+$GRPs. FOV = 160,000 μm^2; n = 5. Statistical analysis was performed using the Mann–Whitney test. Scale bar = 100 μm.

be detected in channels coated with non-activated HBECs, with <10% differences.

Compared to naïve GRPs, we observed a 4-times higher number of VLA-4$^+$GRPs that bound to activated endothelial cells (VLA-4$^+$GRPs 40.4 (95% CI 29.6 to 51.3) compared to naïve GRPs (11.2 (95% CI 6.9 to 16.3; $p = 0.005$; Hedges' $g = 9.6$)) (Figure 3(d)). Taken together, these results indicate that VLA-4$^+$GRPs bind specifically to activated endothelium. Statistical analysis was performed using the Mann–Whitney test.

The effect of VLA-4-transfection on the migratory potential of GRPs

The migratory properties of both naïve GRPs and VLA-4$^+$GRPs were assessed using a microfluidic device with an FBS chemoattractant gradient to drive cell migration. Average cell migration velocity and migration distance into the channels were used as primary readouts. VLA-4$^+$GRPs were found to migrate with moderately higher speeds compared to naïve GRPs, and these differences were statistically significant ($p < 0.001$) in all channel widths except for the 50-μm wide channels, where the speed was 53.4 μm/h (95% CI 43.9 to 62.9) for naïve GRPs and 72.0 μm/h (95% CI 57.4 to 76.6) for VLA4$^+$GRPs ($p = 0.072$). In the 20-μm width channels, VLA-4$^+$GRPs migrated with an average speed of 78.8 (95% CI 72.8 to 84.9) μm/h compared to 44.8 (95% CI 41.5 to 48.1) μm/h for naïve cells ($p < 0.001$; Hedges' $g = 5.914$). In 10-μm wide channels, the speeds were 93.1 (95% CI 86.9 to 99.3) μm/h for VLA-4+GRPs and 53.7 (95% CI 48.8 to 58.7) μm/h for naïve cells ($p < 0.001$; Hedges' $g = 5.845$). In the smallest (6 μm) channel, the average speed changed from 46.3 (95% CI 40.3 to 52.3) μm/h for naïve cells to 85.7 (95% CI 80.7 to 90.7) μm/h for

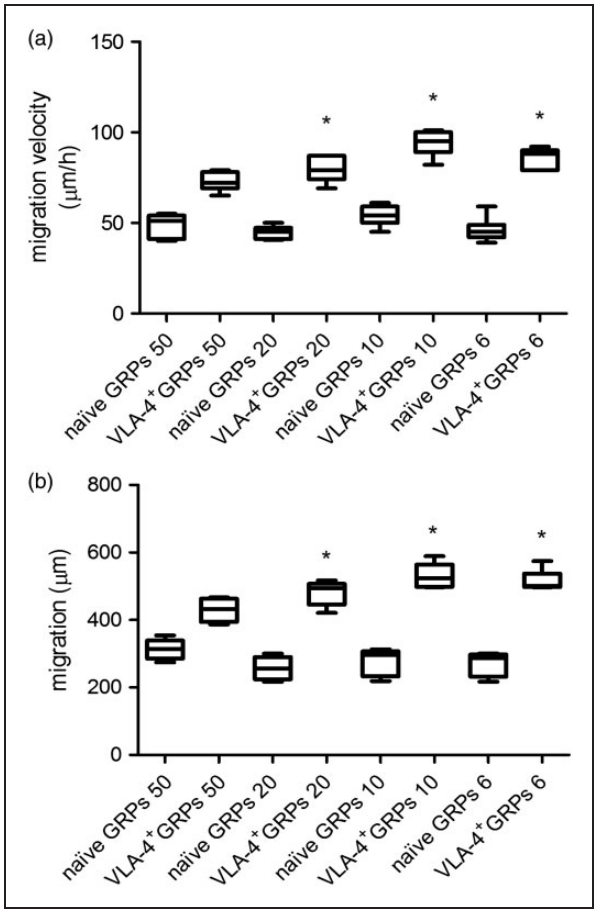

Figure 4. Average migration velocity (a) and migration distance (b) of naïve GRPs and VLA-4$^+$GRPs in response to the FBS chemoattractant gradient in the microchannel migration assay. Asterisk indicates significant differences between the naïve and VLA-4$^+$GRPs. n = 5. Statistical analysis was performed using the Mann–Whitney test.

VLA-4$^+$GRPs ($p < 0.001$; Hedges' $g = 5.752$) (Figure 4(a)). There was also a difference in total distance of cell migration. For 50 μm channels, the total covered distance was higher by 37% (from 312.6 (95% CI 275.5 to 349.7) for naïve cells to 429.2 (95% CI 385.7 to 472.7) for the VLA-4$^+$GRP; $p = 0.008$; Hedges' $g = 3.235$). In the rest of the channel widths, observed differences were larger ($p < 0.001$), reaching 60–70% (20 μm: 257.3 (95% CI 218.7 to 295.8 μm) for naïve GRPs to 480.6 (95% CI 442.4 to 518.8) μm for VLA-4$^+$GRPs (Hedges' $g = 5.518$); 10 μm: 275.4 (95% CI 225.2 to 325.6) μm for naïve GRPs to 530.0 (95% CI 483.5 to 576.5) μm for VLA-4$^+$GRPs (Hedges' $g = 5.9$); 6 μm: 269.4 (95% CI 225.0 to 313.7) μm for naïve GRPs to 514.0 (95% CI 472.2 to 555.7) μm for VLA-4 ± GRPs (Hedges' $g = 6.37$)) (Figure 4(b)). Taken together, our data reveal that VLA-4$^+$GRPs migrate more efficiently in physiologically relevant confined channels and are moderately more efficient in channels resembling a 2D microenvironment when compared to naïve GRPs (Figure 4(b)). The statistical analysis was performed using a Mann–Whitney test.

Homing and diapedesis of GRPs following IA injection in an MCAO mouse model

Multiphoton microscopy of intraarterially transplanted GRPs. MCAO-induced ischemia resulted in increased expression of the VCAM-1 protein on the cerebral endothelium, as detected by immunohistochemistry.[46] Endothelial activation was very rapid, with high VCMA-1 expression detected as early as 24 h after the ischemic insult. At the same time point, IA-injected green fluorescent GRPs were found to adhere to the cerebral endothelium. Compared to naïve cells, the homing of VLA-4$^+$GRPs was more robust. The binding strength of transfected cells was improved, as none of the cells observed over the 3.5-h intravital imaging window detached under the pressure of blood flow. In contrast, binding of naïve GRPs to endothelial cells was not only sparse, but also transient, with cells detaching during imaging and dispersing out of the field of view. Furthermore, time-lapse 2-PM identified multiple examples of infused VLA-4$^+$GRPs extravasating through the blood vessel wall into the brain parenchyma (18% of cells in the field of view) (Figure 5(a)). None of the naïve GRPs showed diapedesis and were either dispersed out from the field of view or remained immobilized inside blood vessels (Figure 5(b)).

Histopathologic confirmation of cell distribution. Histological detection of cells validated the imaging results, demonstrating cells in the ipsilateral hemisphere. For each analyzed region of interest, there were an average of 304.6 (95% CI 234.9 to 374.3) VLA-4$^+$GRPs and 83.0 (95% CI 24.38 to 141.6) of naïve GRPs, indicating an over three-fold higher number of docked cells for VLA-4$^+$ compared to naïve GRPs ($p < 0.001$; Hedges' $g = 3.881$) (Figure 5(c) and (d)). The statistical analysis was performed using the Mann–Whitney test.

Discussion

The safety and feasibility of intraarterial injections have been shown in several animal studies.[47–50] The transplantation of bone marrow mononuclear cells was shown to be safe in Phase I clinical trials in patients with non-acute[51] as well as acute[52] stroke. In both of these studies, no deaths, stroke recurrence, or cell-mediated adverse events were observed during 6 months of follow-up. The safety of intraarterial cell delivery was also shown in Parkinson's patients, where autologous bone marrow mononuclear cells were injected close to the affected area of the brain

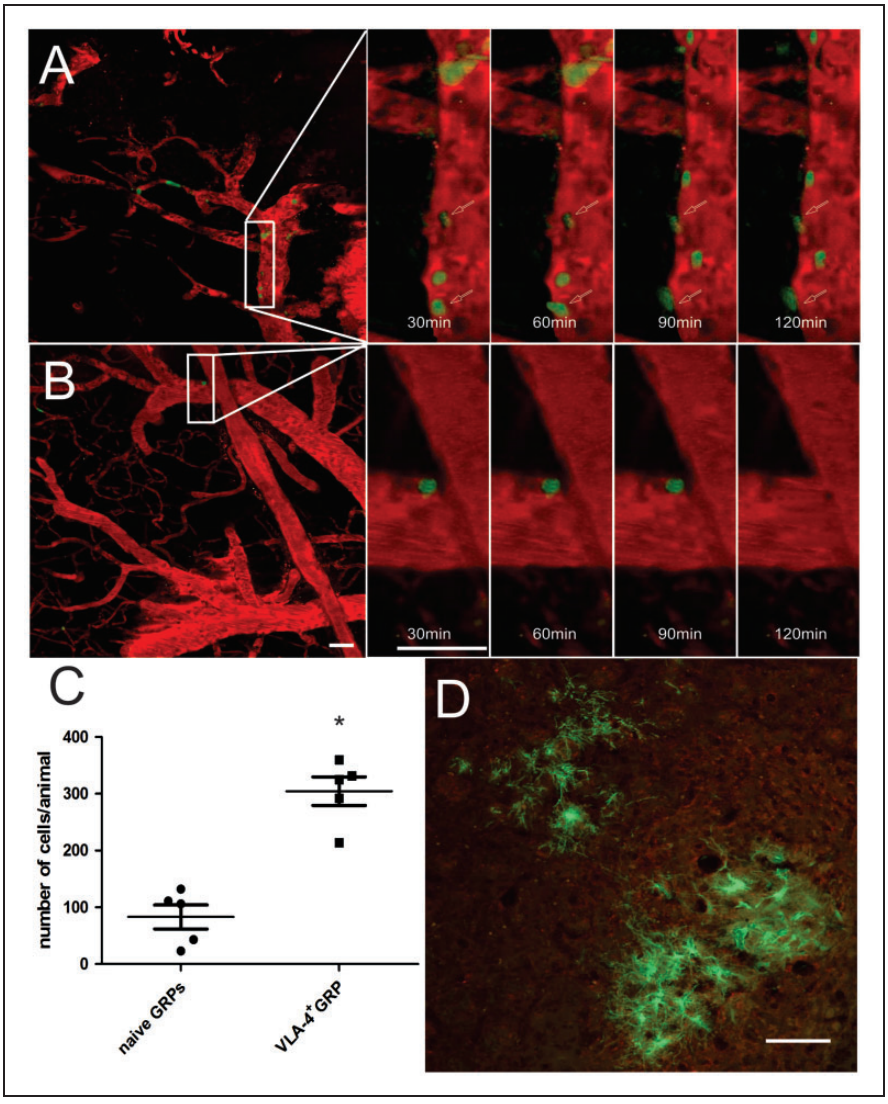

Figure 5. Intravital 2-PM of CMFDA-labeled (green) VLA-4^{+}GRPs (a) and naïve GRPs (b), 24 h after intraarterial delivery in a mouse MCAO model. The number of injected (green) naïve and VLA-4^{+}GRPs, shown as average and 95%CI with each dot representing the mean cell number counted from 20 slices per animal, on the brain slices collected after intra-vital imaging (c) and on brain slices 30 days after IA-injection (d), n = 5. Statistical analysis was performed using the Mann–Whitney test. Scale bar = 100 μm.

with the use of super-selective arterial catheterization.[53] We have previously shown that naïve, immortalized GRPs do not bind to the cerebral endothelium following IA injection, even after global activation with LPS.[37] These small progenitors are not spontaneously captured in the brain and are lost in filtrating organs. In the current study, we have shown that this is also true for the primary, therapeutic GRPs, clearly indicating the need for a strategy that would facilitate their docking and diapedesis. Interestingly, it has been shown that mesenchymal stem cells (MSCs), which are quite large, with a size that exceeds that of the capillary vessels when injected intraarterially, initially localize to the brain, but that homing is transient and usually does not exceed 24 h.[30,54–56] This data suggests that binding of transplanted cells to blood vessel walls is very weak or is based only on passive mechanical trapping in the small vasculature. To increase the efficiency of the endothelial capture of GRPs, we used the well-described VLA-4-VCAM-1 axis involved in the adhesion and extravasation of leukocytes.[57]

Our in vitro studies demonstrate that VLA-4-expressing primary GRPs interact and transiently roll on either recombinant VCAM-1 or activated HBEC cells expressing VCAM-1. VLA-4^{+}GRP cells display a rolling behavior similar to that of leukocytes,[58] confirming the functionality of the transgene. Microfluidic assays have been utilized to study the binding of numerous, functional ligand-receptor pairs, including ligand-P/-E-/L-selectin[40] and ligand-VCAM-1.[58,59] However,

these works do not directly correlate in vitro observations with in vivo results. The interactions of leukocytes with VCAM-1 have been shown to promote rolling and tethering at low shear stresses.[58,59] Also, Vanderslice et al. have shown that the use of a small molecule agonist, which can up-regulate the activity of the α4/β1 heterodimer, greatly enhances the adhesion of Jurkat and endothelial progenitor cells to VCAM-1 under static and flow conditions in a plate, flow-chamber assay. These authors also showed spreading and migration of both kinds of cells after treatment with the VLA-4 agonist.[60] VLA-4 has also been demonstrated to be involved in the migration of cells. It has been shown that the binding of the heterodimer α4/β1 to fibronectin is necessary and sufficient to promote directional cell migration.[61] This is in agreement with results obtained by us from in vitro studies with the use of a microfluidic channel migration assay, where VLA-4$^+$GRPs migrate with higher speeds and travel further than naïve cells. The in vivo VLA-4 expression and the migratory abilities of human melanoma cells have been correlated. Highly metastatic tumor cells were found to express integrins α4/β1 at a high level, whereas non-metastatic melanoma cells displayed a low expression.[62] This indicates that the VLA-4-VCAM-1 axis is not restricted to leukocytes, but can be involved in the migration and diapedesis of other cell types. Here, utilizing in vitro flow-based assays allowed us to verify binding partners using less invasive modes, while still achieving physiologically relevant flow and binding conditions, before proceeding to in vivo validation of VLA-4$^+$GRPs.

After the transplantation of engineered progenitors in an MCAO model of stroke, we observed a significant increase in the number of cells homing to the area of injury. With intravital multi-photon microscopy, we showed a four-fold increase in the number of adhered cells and these observations were validated by histopathology. Although endothelial capture of the transplanted cells is important, and perhaps, sufficient in the case of a paracrine trophic effect, if glial progenitors need to be in close proximity to axons, diapedesis into the brain parenchyma is critical. Several papers have reported some level of migration of the transplanted cells through blood vessel walls after their intravascular delivery. In a rat model of stroke, for the first 24 h after intraarterial injection, MSCs were found inside blood vessels; however, after 10 days, a small number of cells had transmigrated into the brain parenchyma.[31] In another intraarterial delivery study with mannitol-mediated blood–brain barrier disruption, 15% of transplanted pericyte progenitor cells were observed outside the vasculature in the brain parenchyma. However, the majority of cells persisted on the activated endothelial cells in the vessels.[63] Other reports have indicated that intraarterially transplanted cells do not migrate to the brain tissue at all, but remain in the blood vessel lumen.[48,54]

In this context, increasing the diapedesis of transplanted cells is an important issue that warrants further investigation. In the current study, homing of the transplanted cells into injured tissue was observed only after the overexpression of VLA-4. During intravital microscopy, 15% of transplanted cells expressing the integrins α4/β1 migrated through blood vessel walls into the brain parenchyma. The VLA-4/VCAM-1 axis and its role in the diapedesis of transplanted cells have been described by Gavina and co-workers. They showed that the migration of CD133+ stem cells from the vasculature to muscle tissue is dramatically reduced by the VCAM-1 blocking antibody.[64] Another elegant example of manipulating cell trafficking was the intravenous injection of VLA-4-expressing CD34+ cells in tumor-bearing mice. Transplanted cells effectively homed to the tumor (both vascular and parenchymal) and the α4/β1 integrin inhibitor significantly reduced that homing.[65] A similar involvement of the VLA-4/VCAM-1 axis in the homing of stem cells was shown by Brunner and co-workers in virus-induced dilated cardiomyopathy (DCM) where blocking of the VCAM-1 significantly reduced stem cell migration toward the injury and remodeling of the injured heart tissue.[66]

The GRP cells used for this study were extensively tested in animal models and were found to be safe and of high therapeutic potential,[16,17,67] thus clearing a path for their clinical use. Although GRPs are isolated from human fetal brain tissue, and access to that tissue is obviously limited, their potency and safety makes them ideal candidates for initial studies on the feasibility of brain repair in stroke. Nevertheless, our technique of diapedesis enhancement will also be applicable for more plentiful sources of progenitors, such as induced pluripotent stem cells.[68]

In conclusion, our in vitro and in vivo data demonstrate that overexpression of the VLA-4 receptor in progenitor cells, based on DNA plasmid transfection, is a promising strategy with which to increase the efficiency of cell homing after intraarterial transplantation.

Limitations

1. In two-photon microscopy, the imaging window is inherently small, facilitating the observation of only several hundred μm^2 and effective monitoring of only a few cells in the field of view. Tomographic techniques suitable for large-scale imaging, such as MRI, are available; however, the sensitivity and resolution are not suitable for the visualization of diapedesis.

2. Homing of IA-injected cells to the cerebral vasculature and their diapedesis toward the brain parenchyma were higher in VLA-4-overexpressing cells; however, the number of cells that migrated to the brain parenchyma remained small and further improvement of transfection efficiency is needed to facilitate therapeutic applications. As an alternative strategy, the use of mRNA seems to be more promising. mRNA does not carry the risk of insertional mutagenesis and it is also highly effective in non-dividing or primary cells. These qualities make mRNA-based cell engineering highly attractive, particularly for clinical use.[69–71]
3. This work does not include an assessment of the therapeutic effect or functional benefits on stroke-injured mice that is elicited by transplanted progenitors, but was rather focused on improving the endothelial capture and diapedesis of glial progenitor cells

Funding

The author(s) disclosed receipt of the following financial support for the research, authorship, and/or publication of this article: Maryland Stem Cell Research Foundation grants MSCRFF0695, MSCRFII0052, and MSCREFE0714; NIH grants R01 NS076573, R01 NS091110 and R01 CA186286 and Strategmed 1/233209/12/NCBIR/2015.

Acknowledgments

We thank Mary McAllister for editorial assistance.

Declaration of conflicting interests

The author(s) declared no potential conflicts of interest with respect to the research, authorship, and/or publication of this article.

Authors' contributions

Experimental design: AJ, JWMB, MJ, KK, PW; performing experiments and data collection: AJ, DJS, SC, MJ, PW; data processing: AJ, DJS, SC, MJ, PW; manuscript writing and editing: AJ, DJS, SC, JWMB, MJ, KK, PW; final acceptance of the manuscript: AJ, DJS, SC, JWMB, MJ, KK, PW.

References

1. Dickerson LM, Carek PJ and Quattlebaum RG. Prevention of recurrent ischemic stroke. *Am Fam Physician* 2007; 76: 382–388.
2. Luo Y. Cell-based therapy for stroke. *J Neural Transm* 2011; 118: 61–74.
3. Muir KW, Tyrrell P, Sattar N, et al. Inflammation and ischaemic stroke. *Curr Opin Neurol* 2007; 20: 334–342.
4. Espinoza-Rojo M, Iturralde-Rodríguez KI, Chánez-Cárdenas M-E, et al. Glucose transporters regulation on ischemic brain: possible role as therapeutic target. *Cent Nerv Syst Agents Med Chem* 2010; 10: 317–325.
5. Locatelli F, Bersano A, Ballabio E, et al. Stem cell therapy in stroke. *Cell Mol Life Sci* 2009; 66: 757–772.
6. Matute C, Alberdi E, Ibarretxe G, et al. Excitotoxicity in glial cells. *Eur J Pharmacol* 2002; 447: 239–246.
7. Matute C, Alberdi E, Domercq M, et al. Excitotoxic damage to white matter. *J Anat* 2007; 210: 693–702.
8. Park E, Velumian AA and Fehlings MG. The role of excitotoxicity in secondary mechanisms of spinal cord injury: a review with an emphasis on the implications for white matter degeneration. *J Neurotrauma* 2004; 21: 754–774.
9. Stys PK. White matter injury mechanisms. *Curr Mol Med* 2004; 4: 113–130.
10. Itoh K, Maki T, Lok J, et al. Mechanisms of cell–cell interaction in oligodendrogenesis and remyelination after stroke. *Brain Res* 2015; 1623: 135–149.
11. Skoff RP, Bessert DA, Barks JD, et al. Hypoxic-ischemic injury results in acute disruption of myelin gene expression and death of oligodendroglial precursors in neonatal mice. *Int J Dev Neurosci* 2001; 19: 197–208.
12. McIver SR, Muccigrosso M, Gonzales ER, et al. Oligodendrocyte degeneration and recovery after focal cerebral ischemia. *Neuroscience* 2010; 169: 1364–1375.
13. Morrison BM, Lee Y and Rothstein JD. Oligodendroglia: metabolic supporters of axons. *Trends Cell Biol* 2013; 23: 644–651.
14. Wang Y, Piao J-H, Larsen EC, et al. Migration and remyelination by oligodendrocyte progenitor cells transplanted adjacent to focal areas of spinal cord inflammation. *J Neurosci Res* 2011; 89: 1737–1746.
15. Erceg S, Ronaghi M, Oria M, et al. Transplanted oligodendrocytes and motoneuron progenitors generated from human embryonic stem cells promote locomotor recovery after spinal cord transection. *Stem Cells* 2010; 28: 1541–1549.
16. Walczak P, All AH, Rumpal N, et al. Human glial-restricted progenitors survive, proliferate, and preserve electrophysiological function in rats with focal inflammatory spinal cord demyelination. *Glia* 2011; 59: 499–510.
17. Lyczek A, Arnold A, Zhang J, et al. Transplanted human glial-restricted progenitors can rescue the survival of dysmyelinated mice independent of production of mature, compact myelin. *Myelin Exp Neurol* 2017; 291: 74–86.
18. de Paula S, Vitola AS, Greggio S, et al. Hemispheric brain injury and behavioral deficits induced by severe neonatal hypoxia-ischemia in rats are not attenuated by intravenous administration of human umbilical cord blood cells. *Pediatr Res* 2009; 65: 631–635.
19. de Paula S, Greggio S, Marinowic DR, et al. The dose-response effect of acute intravenous transplantation of human umbilical cord blood cells on brain damage and spatial memory deficits in neonatal hypoxia-ischemia. *Neuroscience* 2012; 210: 431–441.
20. Yasuhara T, Matsukawa N, Yu G, et al. Transplantation of cryopreserved human bone marrow-derived multipotent adult progenitor cells for neonatal hypoxic-ischemic injury: Targeting the hippocampus. *Rev Neurosci* 2006; 17: 215–225.

21. Savitz SI, Misra V, Kasam M, et al. Intravenous autologous bone marrow mononuclear cells for ischemic stroke. *Ann Neurol* 2011; 70: 59–69.
22. Savitz SI and Misra V. Launching intravenous bone marrow cell trials for acute stroke. *Regen Med* 2009; 4: 639–641.
23. Fischer UM, Harting MT, Jimenez F, et al. Pulmonary passage is a major obstacle for intravenous stem cell delivery: the pulmonary first-pass effect. *Stem Cells Dev* 2009; 18: 683–692.
24. Janowski M, Walczak P and Date I. Intravenous route of cell delivery for treatment of neurological disorders: a meta-analysis of preclinical results. *Stem Cells Dev* 2010; 19: 5–16.
25. Rosenkranz K, Kumbruch S, Tenbusch M, et al. Transplantation of human umbilical cord blood cells mediated beneficial effects on apoptosis, angiogenesis and neuronal survival after hypoxic-ischemic brain injury in rats. *Cell Tissue Res* 2012; 348: 429–438.
26. Lee JA, Kim B IL, Jo CH, et al. Mesenchymal stem-cell transplantation for hypoxic-ischemic brain injury in neonatal rat model. *Pediatr Res* 2010; 67: 42–46.
27. Donega V, van Velthoven CTJ, Nijboer CH, et al. Intranasal mesenchymal stem cell treatment for neonatal brain damage: long-term cognitive and sensorimotor improvement. *PLoS One* 2013; 8: e51253.
28. Li L, Jiang Q, Ding G, et al. Effects of administration route on migration and distribution of neural progenitor cells transplanted into rats with focal cerebral ischemia, an MRI study. *J Cereb Blood Flow Metab* 2009; 30: 653–662.
29. Misra V, Lal A, El Khoury R, et al. Intra-arterial delivery of cell therapies for stroke. *Stem Cells Dev* 2012; 21: 1007–1015.
30. Cui L-L, Kerkelä E, Bakreen A, et al. The cerebral embolism evoked by intra-arterial delivery of allogeneic bone marrow mesenchymal stem cells in rats is related to cell dose and infusion velocity. *Stem Cell Res Ther* 2015; 6: 11–20.
31. Walczak P, Zhang J, Gilad AA, et al. Dual-modality monitoring of targeted intraarterial delivery of mesenchymal stem cells after transient ischemia. *Stroke* 2008; 39: 1569–1574.
32. Janowski M, Lyczek A, Engels C, et al. Cell size and velocity of injection are major determinants of the safety of intracarotid stem cell transplantation. *J Cereb Blood Flow Metab* 2013; 33: 921–927.
33. Weber C and Springer TA. Interaction of very late antigen-4 with VCAM-1 supports transendothelial chemotaxis of monocytes by facilitating lateral migration. *J Immunol* 1998; 161: 6825–6834.
34. Rosenblum S, Wang N, Smith TN, et al. Timing of intra-arterial neural stem cell transplantation after hypoxia-ischemia influences cell engraftment, survival, and differentiation. *Stroke* 2012; 43: 1624–1631.
35. Gauberti M, Montagne A, Marcos-Contreras OA, et al. Ultra-sensitive molecular MRI of vascular cell adhesion molecule-1 reveals a dynamic inflammatory penumbra after strokes. *Stroke* 2013; 44: 1988–1996.
36. Guzman R, De Los Angeles A, Cheshier S, et al. Intracarotid injection of fluorescence activated cell-sorted CD49d-positive neural stem cells improves targeted cell delivery and behavior after stroke in a mouse stroke model. *Stroke* 2008; 39: 1300–1306.
37. Gorelik M, Orukari I, Wang J, et al. Use of MR cell tracking to evaluate targeting of glial precursor cells to inflammatory tissue by exploiting the very late antigen-4 docking receptor. *Radiology* 2012; 265: 175–185.
38. Phillips AW, Falahati S, DeSilva R, et al. Derivation of glial restricted precursors from E13 mice. *J Vis Exp* 2012; 64: pii: 3462.
39. Tong Z, Cheung LS-L, Stebe KJ, et al. Selectin-mediated adhesion in shear flow using micropatterned substrates: multiple-bond interactions govern the critical length for cell binding. *Integr Biol (Camb)* 2012; 4: 847–856.
40. Shea DJ, Wirtz D, Stebe KJ, et al. Distinct kinetic and mechanical properties govern mucin 16- and podocalyxin-mediated tumor cell adhesion to E- and L-selectin in shear flow. *Oncotarget* 2015; 6: 24842–2455.
41. Hanley J, Barbiere J and Song Y. A clinical procedure for case-specific analytical validation of mono-modality image fusion in image guided radiotherapy. *Conf Proc Annu Int Conf IEEE Eng Med Biol Soc IEEE Eng Med Biol Soc Annu Conf* 2006; 1: 3823–3826.
42. Tong Z, Balzer EM, Dallas MR, et al. Chemotaxis of cell populations through confined spaces at single-cell resolution. *PLoS One* 2012; 7: e29211.
43. Hung W-C, Chen S-H, Paul CD, et al. Distinct signaling mechanisms regulate migration in unconfined versus confined spaces. *J Cell Biol* 2013; 202: 807–824.
44. Balzer EM, Tong Z, Paul CD, et al. Physical confinement alters tumor cell adhesion and migration phenotypes. *FASEB J* 2012; 26: 4045–4056.
45. Sasaki M, Honmou O and Kocsis JD. A rat middle cerebral artery occlusion model and intravenous cellular delivery. *Methods Mol Biol* 2009; 549: 187–195.
46. Justicia C, Martín A, Rojas S, et al. Anti-VCAM-1 antibodies did not protect against ischemic damage either in rats or in mice. *J Cereb Blood Flow Metab* 2006; 26: 421–432.
47. Karlupia N, Manley NC, Prasad K, et al. Intraarterial transplantation of human umbilical cord blood mononuclear cells is more efficacious and safer compared with umbilical cord mesenchymal stromal cells in a rodent stroke model. *Stem Cell Res Ther* 2014; 5: 45–64.
48. Lu S-S, Liu S, Zu Q-Q, et al. In vivo MR imaging of intraarterially delivered magnetically labeled mesenchymal stem cells in a canine stroke model. *PLoS One* 2013; 8: e54963.
49. Zhang L, Li Y, Romanko M, et al. Different routes of administration of human umbilical tissue-derived cells improve functional recovery in the rat after focal cerebral ischemia. *Brain Res* 2012; 1489: 104–112.
50. Janowski M, Walczak P and Pearl MS. Predicting and optimizing the territory of blood-brain barrier opening by superselective intra-arterial cerebral infusion under dynamic susceptibility contrast MRI guidance. *J Cereb Blood Flow Metab* 2016; 36: 569–575.

51. Battistella V, de Freitas GR, da Fonseca LMB, et al. Safety of autologous bone marrow mononuclear cell transplantation in patients with nonacute ischemic stroke. *Regen Med* 2011; 6: 45–52.
52. Rosado-de-Castro PH, Schmidt F, da R, Battistella V, et al. Biodistribution of bone marrow mononuclear cells after intra-arterial or intravenous transplantation in subacute stroke patients. *Regen Med* 2013; 8: 145–155.
53. Brazzini A, Cantella R, de la Cruz A, et al. Intraarterial autologous implantation of adult stem cells for patients with Parkinson disease. *J Vasc Interv Radiol* 2010; 21: 443–451.
54. Mitkari B, Kerkelä E, Nystedt J, et al. Intra-arterial infusion of human bone marrow-derived mesenchymal stem cells results in transient localization in the brain after cerebral ischemia in rats. *Exp Neurol* 2013; 239: 158–162.
55. Khabbal J, Kerkelä E, Mitkari B, et al. Differential clearance of rat and human bone marrow-derived mesenchymal stem cells from the brain after intra-arterial infusion in rats. *Cell Transplant* 2015; 24: 819–828.
56. Nemeth CL, Shurte MS, McTigue DM, et al. Microembolism infarcts lead to delayed changes in affective-like behaviors followed by spatial memory impairment. *Behav Brain Res* 2012; 234: 259–266.
57. Mitroulis I, Alexaki VI, Kourtzelis I, et al. Leukocyte integrins: Role in leukocyte recruitment and as therapeutic targets in inflammatory disease. *Pharmacol Ther* 2015; 147C: 123–135.
58. Alon R, Kassner PD, Carr MW, et al. The integrin VLA-4 supports tethering and rolling in flow on VCAM-1. *J Cell Biol* 1995; 128: 1243–1253.
59. Alon R, Fuhlbrigge RC, Finger EB, et al. Interactions through L-selectin between leukocytes and adherent leukocytes nucleate rolling adhesions on selectins and VCAM-1 in shear flow. *J Cell Biol* 1996; 135: 849–865.
60. Vanderslice P, Biediger RJ, Woodside DG, et al. Small molecule agonist of very late antigen-4 (VLA-4) integrin induces progenitor cell adhesion. *J Biol Chem* 2013; 288: 19414–19428.
61. Dikeman DA, Rivera Rosado LA, Horn TA, et al. α4 β1-Integrin regulates directionally persistent cell migration in response to shear flow stimulation. *Am J Physiol Cell Physiol* 2008; 295: C151–C159.
62. Klemke M, Weschenfelder T, Konstandin MH, et al. High affinity interaction of integrin alpha4beta1 (VLA-4) and vascular cell adhesion molecule 1 (VCAM-1) enhances migration of human melanoma cells across activated endothelial cell layers. *J Cell Physiol* 2007; 212: 368–374.
63. Youn SW, Jung K-H, Chu K, et al. Feasibility and safety of intraarterial pericyte progenitor cell delivery following mannitol-induced transient blood–brain barrier opening in a canine model. *Cell Transplant* 2015; 24: 1469–1479.
64. Gavina M, Belicchi M, Rossi B, et al. VCAM-1 expression on dystrophic muscle vessels has a critical role in the recruitment of human blood-derived CD133+ stem cells after intra-arterial transplantation. *Blood* 2006; 108: 2857–2866.
65. Jin H, Aiyer A, Su J, et al. A homing mechanism for bone marrow-derived progenitor cell recruitment to the neovasculature. *J Clin Invest* 2006; 116: 652–662.
66. Brunner S, Theiss HD, Leiss M, et al. Enhanced stem cell migration mediated by VCAM-1/VLA-4 interaction improves cardiac function in virus-induced dilated cardiomyopathy. *Basic Res Cardiol* 2013; 108: 388–402.
67. Windrem MS, Nunes MC, Rashbaum WK, et al. Fetal and adult human oligodendrocyte progenitor cell isolates myelinate the congenitally dysmyelinated brain. *Nat Med* 2004; 10: 93–97.
68. Wang S, Bates J, Li X, et al. Human iPSC-derived oligodendrocyte progenitor cells can myelinate and rescue a mouse model of congenital hypomyelination. *Cell Stem Cell* 2013; 12: 252–264.
69. Yamamoto A, Kormann M, Rosenecker J, et al. Current prospects for mRNA gene delivery. *Eur J Pharm Biopharm Off J Arbeitsgemeinschaft fuür Pharm Verfahrenstechnik eV* 2009; 71: 484–489.
70. Phua KKL, Leong KW and Nair SK. Transfection efficiency and transgene expression kinetics of mRNA delivered in naked and nanoparticle format. *J Control Release* 2013; 166: 227–233.
71. Youn H and Chung J-K. Modified mRNA as an alternative to plasmid DNA (pDNA) for transcript replacement and vaccination therapy. *Expert Opin Biol Ther* 2015; 15: 1337–1348.